Icarus 246 (2015) 213–219

Contents lists available at ScienceDirect

Icarus

journal homepage: www.elsevier.com/locate/icarus

Spectral variability of Charon's 2.21-μm feature

Francesca E. DeMeo [a,b,*], Christophe Dumas [c], Jason C. Cook [d], Benoit Carry [e], Frederic Merlin [f,g], Anne J. Verbiscer [h], Richard P. Binzel [b]

[a] Harvard-Smithsonian Center for Astrophysics, 60 Garden Street, MS-16, Cambridge, MA 02138, USA
[b] Department of Earth, Atmospheric, and Planetary Sciences, Massachusetts Institute of Technology, 77 Massachusetts Avenue, Cambridge, MA 02139, USA
[c] European Southern Observatory, Alonso de Cordova 3107, Vitacura, Casilla 19001, Santiago 19, Chile
[d] Southwest Research Institute, 1050 Walnut St. Suite 300, Boulder, CO 80302, USA
[e] Institut de Mécanique Céleste et de Calcul des Éphémérides, Observatoire de Paris, UMR8028 CNRS, 77 av. Denfert-Rochereau, 75014 Paris, France
[f] LESIA, Observatoire de Paris, F-92195 Meudon Principal Cedex, France
[g] Université Denis Diderot, Sorbonne Paris Cité, 4 rue Elsa Morante, 75205 Paris Cedex 13, France
[h] Department of Astronomy, University of Virginia, Charlottesville, VA 22904-4325, USA

ARTICLE INFO

Article history:
Received 19 December 2013
Revised 21 March 2014
Accepted 12 April 2014
Available online 28 April 2014

Keywords:
Charon
Spectroscopy
Ices
Kuiper Belt

ABSTRACT

The clear angular separation of Pluto and Charon from ground-based telescopes has been enabled by improved technology, particularly adaptive optics systems. Near-infrared spectral data have revealed Charon's surface to be rich in crystalline water ice and ammonia hydrates. In this work, we search for spectral differences across Charon's surface with new near-infrared spectral data taken in the *K*-band (2.0–2.4 μm) with SINFONI on the VLT and NIRI on Gemini North as well as with previously published spectral data. The strength of the absorption band of ammonia hydrate is dependent on the state of the ice, concentration in H_2O, grain size, temperature and exposure to radiation. We find variability of the band center and band depth among spectra. This could indicate variability of the distribution of ammonia hydrate across Charon's surface. If the spectral variation is due to physical properties of Charon, the New Horizons flyby could find the concentration of ammonia hydrate heterogeneously distributed across the surface. Comparison between this work and New Horizons results will test the limits of ground-based reconnaissance.

1. Introduction

Charon is the largest moon of the dwarf planet Pluto, located at Neptune's 3:2 mean-motion resonance in the Kuiper Belt. At the time of the Pluto–Charon mutual eclipse events (while the orbital plane of Pluto and Charon was aligned with the line-of-sight from Earth from 1985 until 1990), observers were able to distinguish color and compositional differences between Pluto and Charon, identifying H_2O-ice on Charon's surface (Buie et al., 1987; Marcialis et al., 1987; Binzel, 1988). The first spectra that could clearly separate Charon's light from Pluto without the aid of occultation revealed a surface rich in crystalline water–ice (Brown and Calvin, 2000; Buie and Grundy, 2000; Dumas et al., 2001). A weak feature detected at 2.21 μm is also present on the surface and is suggested to be due to ammonia hydrate (Brown and Calvin, 2000; Buie and Grundy, 2000; Dumas et al., 2001; Cook et al., 2007; Verbiscer et al., 2007). An additional weak feature at 2.0 μm assumed to also be due to the presence of ammonia hydrate was detected by Merlin et al. (2010).

Charon can be compared with mid-size Transneptunian Objects (TNOs) in the 1000 km diameter size range. A handful of TNOs display prominent features at 1.5, 1.65, and 2.0 μm indicating a surface dominated by crystalline water–ice including Orcus (Fornasier et al., 2004; de Bergh et al., 2005), Quaoar (Jewitt and Luu, 2004), and Haumea (Trujillo et al., 2007; Dumas et al., 2011). Many icy satellites of the outer planets also have water–ice features (e.g., Calvin et al., 1995; Grundy et al., 1999, 2006; Clark et al., 2013). The best spectral analogs to Charon are the medium-sized TNO Orcus and the Saturnian satellite Tethys that, like Charon, have a distinct absorption feature at 2.21 μm (de Bergh et al., 2005; Barucci et al., 2008; Verbiscer et al., 2008).

Each spectrum that has been measured thus far provides a glimpse of the characteristics of a specific part of Charon's surface. Cook et al. (2007) find differences in the band position at 2.21 μm suggesting different ammonia hydration states across the surface. Dumas et al. (2001) detect the feature associated with ammonia

* Corresponding author at: Harvard-Smithsonian Center for Astrophysics, 60 Garden Street, MS-16, Cambridge, MA 02138, USA.
E-mail address: fdemeo@cfa.harvard.edu (F.E. DeMeo).

http://dx.doi.org/10.1016/j.icarus.2014.04.010
0019-1035/

on the leading side of Charon, but not the trailing side. Buie and Grundy (2000) measure four spectra across the surface and find weak spatial variation of H_2O ice, with stronger absorption on the leading hemisphere. They also note a neutrally absorbing component past 2 μm similar to that seen on icy outer Solar System satellites.

In this work we present new near-infrared spectral data at 3 locations on Charon's surface from SINFONI on the Very Large Telescope (VLT) and 1 from the Near InfraRed Imager (NIRI) on Gemini North. We compare all high spectral resolution, high signal-to-noise ratio data available of Charon to determine how the 2.21 μm feature varies across the surface.

2. Observations

Here we present new near-infrared spectral data at 4 locations on Charon's surface, 3 from SINFONI on the VLT and 1 from NIRI on Gemini North. Previously published data included in this work are from Brown and Calvin (2000), Buie and Grundy (2000), Dumas et al. (2001), Cook et al. (2007), Verbiscer et al. (2007), Merlin et al. (2010). Observing and reduction information is contained therein. Below we describe observation and data reduction procedures for unpublished data.

2.1. SINFONI, VLT

Observations of Charon and Pluto were performed using the SINFONI instrument (Spectrograph for INtegral Field Observations in the Near Infrared), installed at the 8.2-m European Southern Observatory (ESO) VLT, Unit 4 at Paranal Observatory. As described in Dumas et al. (2007) SINFONI is an image slicer integral field spectrometer (Eisenhauer et al., 2003; Bonnet et al., 2004) with a field-of-view split into 32 image-slitlets that reflect onto small plane mirrors before being re-directed toward the selected grating. The 32 spectra are then re-imaged on a 2048 × 2048 pixel Hawaii 2RG (1–2.5 μm) near-infrared detector. We used the $H + K$ spectral grating (resolving power $R \sim 1500$) covering both H and K bands simultaneously (1.4–2.4 μm), and a spatial scale of 12.5 × 25 mas/spaxel (0.8″ × 0.8″ field-of-view). With this small field-of-view, we were able to take separate observations of Pluto and Charon.

Data were taken on May 13, June 9, and August 9, 2005. Total exposure times for each night were 5 min for Pluto and 25 min for Charon (the analysis of Pluto was published in DeMeo et al. (2010)). Observations were taken under clear sky conditions, at airmasses less than 1.15 and seeing generally one arcsecond or less. Solar analogs were observed each night to correct for telluric features. The detector was aligned in the Pluto–Charon direction. For observational conditions and circumstances, see Table 1. For the coordinates reported, the north pole follows the angular momentum vector and the sub-Earth longitude is zero at the sub-Charon (or sub-Pluto) point and decreases in time, following the IAU recommendation (Archinal et al., 2011).

Reduction was performed using the ESO SINFONI pipeline combined with custom IDL procedures. First the data were corrected for bad lines created from bad pixels located among the four non-illuminated edge pixels at the beginning and end of each row. Master darks, master flats, bad pixel maps, and wavemaps were created within the SINFONI pipeline. We improved the master bad pixel map by combining the pipeline output with a more sensitive map created from an IDL routine. Xe–Ar–Kr lamps were used for wavelength calibration, and as part of the SINFONI pipeline, a wavelength map was computed to derive a direct correspondence between pixel position and wavelength. Determining the orientation and position of each spectrum on the detector enabled the reconstruction of an image-cube of the original field-of-view. A sky spectrum was taken nearby before or after observing the object to correct for sky background.

The slices within each image cube were then realigned using an IDL routine that calculated the location of the maximum signal using a 2-D gaussian and shifting it to a center pixel. This alignment allows a smaller aperture to be used when extracting the spectra. We extracted test spectra before and after alignment to be confident that the alignment did not introduce artifacts to the data. A second sky correction was performed by finding the median sky value for each slice within an annulus after rejecting the highest and lowest 10%, and subtracting that median value from the entire slice. The spectra were then extracted from the individual data cubes using QFitsView, the 3D-visualisation tool developed at the Max Planck Institute for Extraterrestrial Physics (MPE) for SINFONI.[1] The individual spectra were corrected for the remaining bad pixels and divided by the solar analog spectra. The Charon data, having more than one spectrum per night, were then combined and normalized to the mean value between 1.7 and 1.75 μm.

2.2. NIRI, Gemini

Charon was also observed with the 8-m Gemini telescope on Mauna Kea. K-band (2.0–2.4 μm, $R \sim 600$) spectra were obtained on 2008 May 30, June 5, and June 18 UT with NIRI (Hodapp et al., 2003) with the Altair adaptive optics (AO) system. The data were reduced using in-house IDL programs. Prior to extracting the 1-D spectrum, the data were pretreated to remove several electronic patterns. These patterns become more apparent when the data are read-noise limited. We removed three patterns: (i) bias offsets, (ii) banding and (iii) striping. The bias differences were estimated by taking the median of the unilluminated portion of each quadrant. The four median values were averaged and a constant was added to each quadrant so the median background equals the average value. Banding is a 16-pixel wide pattern seen in the spectral images that runs perpendicular to the spectrum. The pattern is measured in each quadrant and removed. Striping is an alternating pattern that is parallel to the spectrum. The intensity of the alteration is sensitive to the flux incident on a given pixel. This striping pattern was measured in each quadrant and removed.

The extraction of the 1-D spectrum generally followed the method of optimal extraction by Horne (1986). This method is most useful in the extraction of low signal-to-noise (SNR) data and can result in a final SNR that is equivalent to a 70% increase in the exposure time. Our optimal extraction routine used estimates for the read-noise (10 e^-), dark current (0.75 e^-/s/pix) and gain (12.3 e^-/ADU) to produce errors for each point of the array. The errors were then used to weight each pixel and then the spectrum was extracted from the image.

The method of extraction diverged from Horne (1986) for sky subtraction. Instead of modeling the sky after masking out the objects' spectral beam, we used a 2-D spectrum of the objects at the opposite dither position. By analyzing image differences, we accurately removed dark current and most of the sky flux. However, the difference image had a read-noise $\sqrt{2}$ greater than a single spectral image. Since the data were not read-noise limited, the greater read noise had a minor adverse impact on the final spectrum.

To maximize the effect of optimal extraction, it is important to map out the location of the spectral beam, known as the trace, in the 2-D image. We estimated the trace of the object by finding the maximum signal in each column, and fit a third order polyno-

[1] http://www.mpe.mpg.de/~ott/QFitsView.

Table 1
Observational circumstances for 2.21 μm absorption feature measurements on Charon.

Date (UT)	Time (UT)	Angular separation[a]	Sub-Earth point[b]		2.21 μm Band parameters				Instrument	Author
			Long.	Lat.	Center	Depth	Width	Area		
1998 March 17	19:10	0.7	234	24	–	–	–	–	HST NICMOS	Buie and Grundy (2000)
1998 March 27	12:00	0.7	48	24	–	–	–	–	HST NICMOS	Buie and Grundy (2000)
1998 May 28	19:10	0.5	334	24	–	–	–	–	HST NICMOS	Buie and Grundy (2000)
1998 June 07	7:10	0.7	321	22	–	–	–	–	HST NICMOS	Buie and Grundy (2000)
1998 June 11	13:01	0.9	82	22	–	–	–	–	HST NICMOS	Dumas et al. (2001)
1998 June 14	14:56	0.9	268	22	–	–	–	–	HST NICMOS	Dumas et al. (2001)
1999 May 28	10:20	0.8	358	26	–	–	–	–	Keck NIRC	Brown and Calvin (2000)
2005 May 2	7:36	0.8	59	37	–	–	–	–	Magellan CorMASS	Verbiscer et al. (2007)
2005 May 13	6:37	0.6	161	37	2.2093 ± 0.0010	−0.0418 ± 0.0047	0.0176 ± 0.0025	0.00078 ± 0.00014	VLT SINFONI	This work
2005 June 09	3:22	0.9	88	36	2.2093 ± 0.0015	−0.0238 ± 0.0041	0.0187 ± 0.0041	0.00047 ± 0.00013	VLT SINFONI	This work
2005 August 09	23:14	0.6	203	35	2.2090 ± 0.0008	−0.0515 ± 0.0044	0.0203 ± 0.0022	0.00111 ± 0.00015	VLT SINFONI	This work
2005 August 26	5:19	0.7	7	35	2.2072 ± 0.0004	−0.0615 ± 0.0030	0.0149 ± 0.0009	0.00097 ± 0.00008	Gemini NIRI	Cook et al. (2007)
2005 September 11	5:16	0.5	185	37	2.2088 ± 0.0003	−0.0734 ± 0.0028	0.0189 ± 0.0009	0.00148 ± 0.00009	Gemini NIRI	Cook et al. (2007)
2008 April 12	9:40	0.8	243	42	2.2116 ± 0.0015	−0.0513 ± 0.0086	0.0186 ± 0.0039	0.00102 ± 0.00027	VLT SINFONI	Merlin et al. (2010)
2008 April 13	8:40	0.6	188	42	2.2095 ± 0.0008	−0.0482 ± 0.0038	0.0218 ± 0.0022	0.00112 ± 0.00014	VLT SINFONI	Merlin et al. (2010)
2008 May 30[c]	12:52	0.8	50	42	2.2078 ± 0.0010	−0.0365 ± 0.0032	0.0224 ± 0.0026	0.00087 ± 0.00013	Gemini NIRI	This work
2008 June 05[c]	12:26	0.9	73	42	"	"	"	"	Gemini NIRI	This work
2008 June 18[c]	10:19	0.8	65	41	"	"	"	"	Gemini NIRI	This work

[a] The angular separation between Charon and Pluto in arc sec.
[b] For the coordinates reported, the north pole follows the angular momentum vector and the sub-Earth longitude is zero at the sub-Charon (or sub-Pluto) point and decreases in time.
[c] The spectra from May and June 2008 were combined and analyzed as one.

mial to a standard star spectrum. The coefficients for the high (greater than zeroth) terms were applied to the spectral image of Pluto and Charon and the zeroth order term was determined from the profile of each object.

We determined the wavelength calibration by identifying night sky lines. We estimated that the wavelength calibration is accurate to 0.03 and 0.10 pixels (with a wavelength dispersion of 7.09 Å/pix), depending on the spectrum and wavelength. The standard star observations, which ranged in airmasses similar to the observations of Charon, were used to model the telluric and solar absorption spectrum at the airmass of the Charon observations. These models were used to convert the Charon spectra to albedo, correct for telluric and solar absorption and correct for instrument response by dividing Charon by the model. A weighted average spectrum of Charon was then obtained. Additional data of Charon taken with NIRI in 2005 used in this work were first analyzed in Cook et al. (2007).

2.3. CorMASS, Magellan

Charon's near-infrared spectrum (0.8–2.5 μm) was measured on May 2, 2005 with the spectrometer CorMASS ($R \sim 300$) while it was a visiting instrument at the 6.5-m Magellan telescope at Las Campanas Observatory in Chile. Even without adaptive optics, Pluto and Charon were spatially resolved in the CorMASS slit because their separation was ~0.8″ and the seeing was ~0.4″ at the time of data acquisition. Although Pluto and Charon were spatially resolved in the CorMASS slit, Charon's spectrum was minimally contaminated by flux from Pluto. To remove this contamination, we subtracted 2.5% of Pluto's flux from that of Charon. These data were originally reported in Verbiscer et al. (2007).

3. Results

To calculate band parameters for the absorption feature at 2.21 μm we use an IDL program created by Carry et al. (2011) and designed to fit Gaussians to potential features in designated wavelength regions. A least squares minimization (Markwardt, 2009) is used to find the best-fit center, width, and depth of the bands. The results of the Gaussian fits to the 2.21 μm band are listed in Table 1, and plots of the fits are shown in Fig. 1.

While the 2.21 μm band is clearly detectable in the data published by Brown and Calvin (2000), Buie and Grundy (2000), Dumas et al. (2001), Verbiscer et al. (2007), the low resolution ($R \leqslant 300$) and signal-to-noise ratios (SNR) are not sufficient to characterize the band at a level of detail comparable with higher spectral resolution data discussed in this paper. Nonetheless, taken together, all of the observations allow us to confirm the presence of the band at all measured locations (Fig. 2).

The 2.21 μm band can be confidently characterized for the higher spectral resolution and high SNR data published in Cook et al. (2007), Merlin et al. (2010), and this work. The band center, depth, area, and width are plotted with their 1-σ error bars in Fig. 3. While the band centers for the leading and anti-Pluto sides of Charon are all consistent, the center is at a shorter wavelength on the sub-Pluto side compared with anti-Pluto. The band center

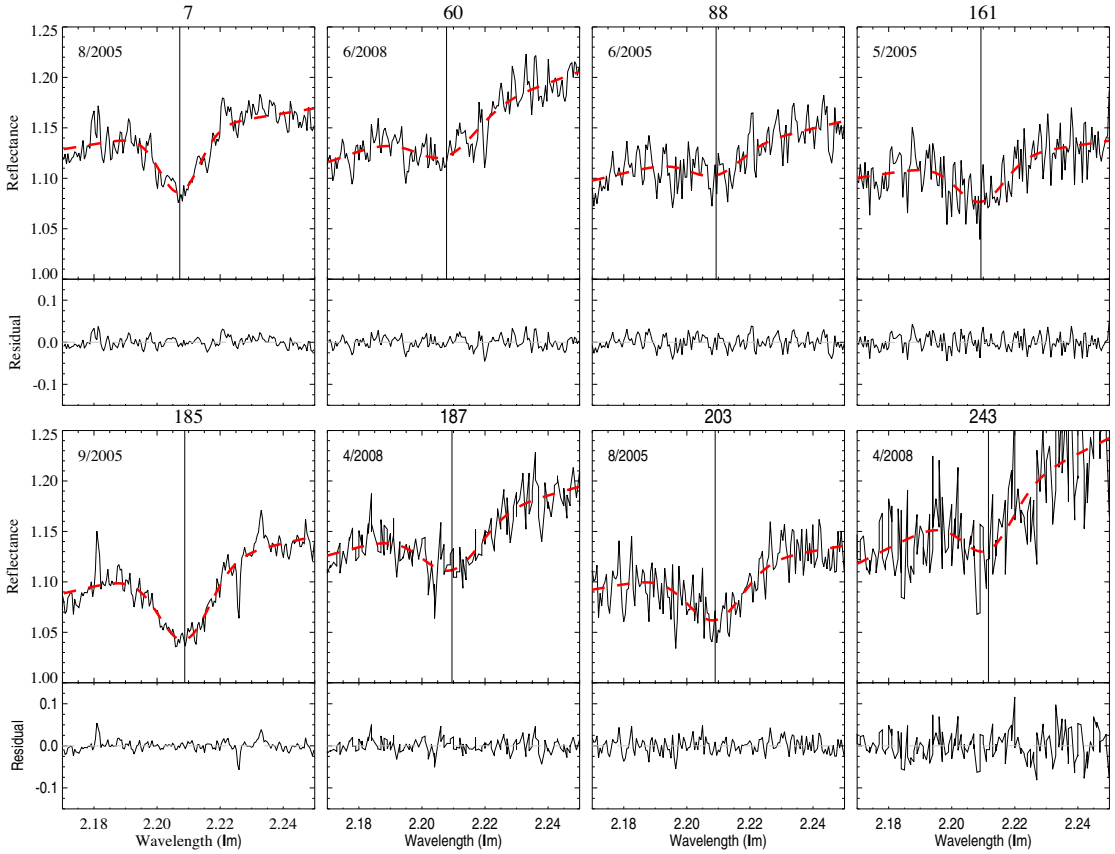

Fig. 1. Near-infrared measurements of Charon in the 2.2 μm spectral region obtained by SINFONI on the VLT and NIRI on Gemini North over the years 2005 to 2008. The measured spectral data are in black with gaussian fits drawn as a red, dashed line, with these fit values reported in Table 1. The vertical line marks the position of the band center. The bottom panel of each plot shows the residual of the gaussian subtracted from the data. The observation date and longitude at which each spectrum was taken are marked at the top of each plot. Differences in the characteristics of the band are visually apparent. The spectrum marked at longitude 60 is a combination of three spectra near that location (see Table 1). (For interpretation of the references to color in this figure legend, the reader is referred to the web version of this article.)

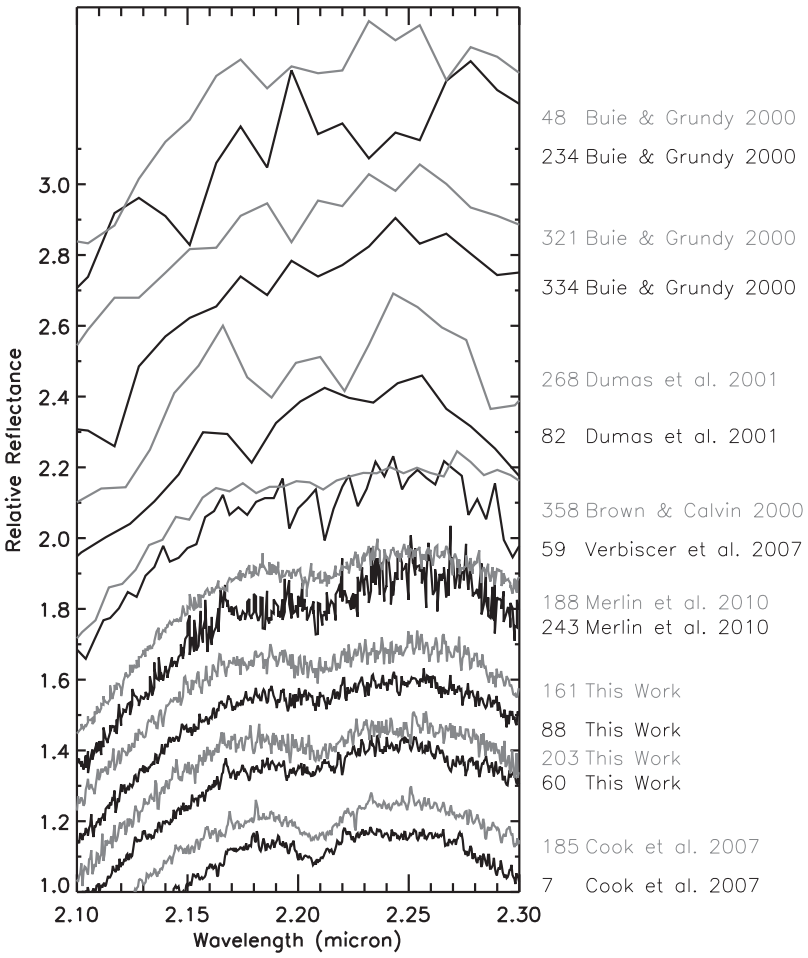

Fig. 2. Direct comparison of multi-longitude measurements on Charon in the 2.2 μm spectral region offset for clarity. The longitude and data reference for each spectrum is marked on the right of the figure (also noted in Table 1). Black and gray colors are for clarity. Variations in the presence or near-absence of the 2.21 μm feature are apparent among the sampled longitudes. The spectrum marked at longitude 60 is a combination of three spectra near that location (see Table 1).

for the measurement taken at a longitude of 7 degrees differs from the mean by >4σ and two other points differ by >1σ. The band center for the trailing side is at a longer wavelength than the other spectra, although the error bar for that point is larger. If the trend is true, then the band center increases with increasing longitude and we would expect the band center to decrease from longitudes 270 to 360 where we have no data of sufficient quality. Cook et al. (2007) find a significant band center difference between the spectra taken on Charon's sub-Pluto (2.1995 μm) and anti-Pluto surface (2.2131 μm). A new reduction and analysis performed in this work reveals that the band center of the sub-Pluto data from Cook et al. (2007) is much closer to the values for the other spectra in this work, though it is still positioned at the shortest wavelength. If this datapoint is excluded, the argument for band center variability is substantially reduced.

The FWHM (full width at half maximum) is roughly consistent among all data within the errors except for the datapoint on the sub-Pluto side that is significantly narrower than most points (>4σ from the mean). The band area is related to the band width and depth so we do not discuss band area separately. We find the band depth reaches a minimum between longitudes of 90 and 180 and stays relatively constant throughout the rest of the surface. The three data points between 0° and 90° longitude differ from the mean by >8, 3, and 6σ, respectively. Of the three measurements taken near 180°, one has a significantly greater depth. At this location the band depth increases from the May to September 2005 measurements and then decreases in the 2008 measurement. It seems unlikely that such a notable change could be caused by physical changes on such a short timescale. While plausible scenarios exist for increasing the amount of ammonia hydrate on the surface, ammonia hydrate cannot be destroyed on such short timescales (Moore et al., 2007). The data clearly indicate spectral variability, however, with the small size of the current dataset we cannot be certain this variability is due to real physical properties or is due to artifacts unaccounted for from the measurement or reduction process. For example, one possible explanation for the depth discrepancy is there could potentially be contamination by methane from Pluto at that band position increasing the band depth, although contamination was not seen in the analysis by Cook et al. (2007) and all the other band parameters for that spectrum are consistent with other measurements here.

In the case that the changes in the spectral features are due to physical properties of Charon's surface, we investigate the meaning of the variability through spectral models. To test the effects of concentration of NH_3 diluted in H_2O (1% and 3% NH_3:H_2O) and grain size on the 2.21-μm band we create multiple synthetic spectra based on radiative transfer models (Hapke, 1981) using optical constants derived in Bauer et al. (2002) based on data by Brown et al. (1988). The optical constants were derived using the technique from Clark and Roush (1984). The band depth is affected by both concentration and grain size. Our measured results are most consistent with 1% concentration. Grain size typically affects band depth (large grains cause deeper absorptions), so we model a range of grain sizes (30–180 μm). The models created from

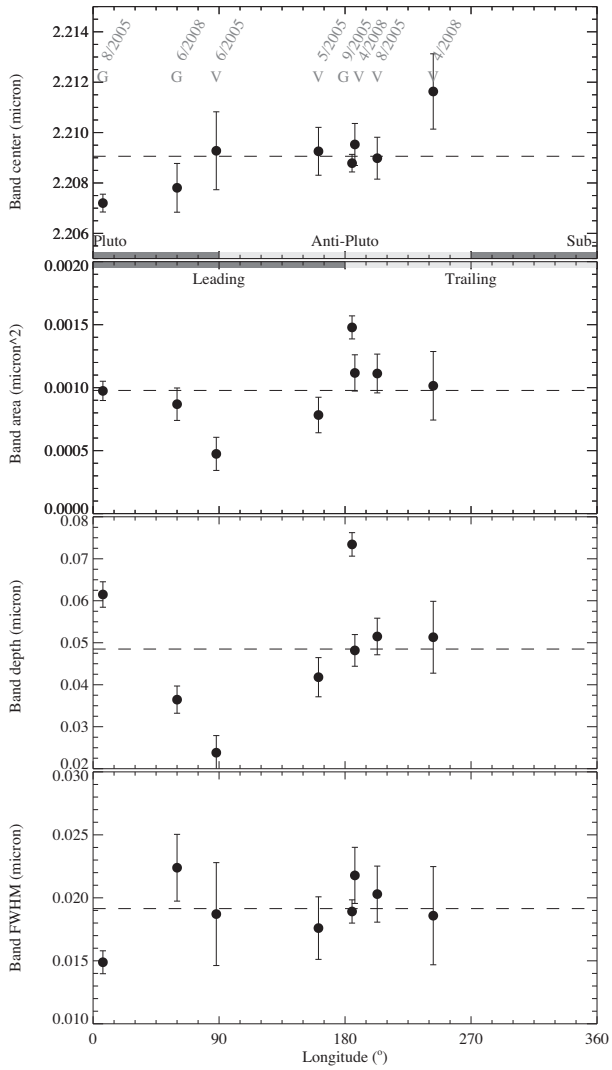

Fig. 3. Measured characteristics of the 2.21 μm spectral feature on Charon as a function of sub-Earth longitude at the time of the observation. The date of each observation is marked in the top panel. "G" marks spectra taken on Gemini and "V" marks spectra taken on the VLT. The horizontal dashed line represents the mean of the eight values. Note that the band area is related to the band depth and FWHM, it is not an independent variable.

different grain sizes result in band depths that span the entire range of measured depths in our observational data. The FWHM is relatively unchanged when varying concentration and grain size and all the models are consistent with our measurements thus providing no additional constraints. We find the band center is unaffected by grain size, but that the band center shifts to longer wavelengths with higher concentrations of ammonia hydrate, as shown in laboratory work by Moore et al. (2007). The band centers we measure are in fact at even shorter wavelengths than for the 1% concentration model.

Laboratory work suggests that the shift in band center with longitude could indicate varying concentrations of ammonia hydrate (Moore et al., 2007). The variations seen in band depth could be due either to changes in concentration or grain size or both. It is not necessary to include any other additional chemical compound to explain the characteristics of the 2.21-μm absorption band, but we cannot rule out the possibility. The band characteristics also change as a function of temperature, irradiation, and hydration state (along with mixtures of ammonia and water, there are three types of ammonia hydrates; dihydrate $NH_3{\cdot}2H_2O$, monohydrate $NH_3{\cdot}H_2O$, and hemihydrate $2NH_3{\cdot}H_2O$, Strazzulla and Palumbo, 1998; Moore et al., 2007), however there is not sufficient information available about these different states to distinguish their effects.

Because ammonia hydrate is not stable on the surface of medium-sized icy bodies such as Charon, cryovolcanism and solid state convection are two plausible mechanisms (Cook et al., 2007) to replenish ammonia hydrate on the surface from the interior. If this is true, then the variation of Charon's 2.21 μm band may allow identification of more or less geologically active regions of the surface. For example, if the spectral differences are due to physical properties of Charon's surface, it is possible that the regions where measured spectra have deeper bands are more active and have recently exposed ammonia hydrate to the surface.

4. Conclusion

Near-infrared spectra acquired at various locations on Charon's surface show that a band at 2.21 μm attributed to ammonia hydrate is ubiquitous. We find that the band depth and center vary across Charon's surface although the FWHM remains relatively constant. If the spectral variability is due to physical properties, the regions with band centers at longer wavelengths likely have higher concentrations of ammonia hydrate. Regions with deeper bands could also be due to higher concentrations if linked with band centers at longer wavelengths. In regions where the deeper band is not correlated with longer wavelength band centers, the depth could be due to larger grain sizes. Because of the limited available ground-based data, we cannot be certain the spectral variability is due to real physical surface properties as opposed to unaccounted for artifacts in the observing and reduction process. These data will serve as test for the limits of ground-based reconnaissance. The detailed maps that will be created from the New Horizons flyby in 2015 will shed light on the Charon's surface properties and whether they vary across the surface.

Acknowledgments

We thank Mike Brown, Marc Buie, and Will Grundy for sharing their data. We thank Amanda Zangari for help understanding coordinate systems. We acknowledge Rosario Brunetto for helpful discussions and two anonymous referees for valuable comments. This work is based on observations performed at the European Southern Observatory (ESO) under Programs 075.C-0434 and 178.C-0036. Support for this work was provided by NASA through Hubble Fellowship grant HST-HF-51319.01-A awarded by the Space Telescope Science Institute, which is operated by the Association of Universities for Research in Astronomy, Inc., for NASA, under contract NAS 5-26555. This material is based upon work supported by the National Aeronautics and Space Administration under Grant No. NNX12AL26G issued through the Planetary Astronomy Program and by the National Science Foundation under Grant 0907766. Any opinions, findings, and conclusions or recommendations expressed in this article are those of the authors and do not necessarily reflect the views of the National Aeronautics and Space Administration or the National Science Foundation.

References

Archinal, B.A. et al., 2011. Report of the IAU working group on cartographic coordinates and rotational elements: 2009. Celest. Mech. Dynam. Astron. 109, 101–135.
Barucci, M.A. et al., 2008. Surface composition and temperature of the TNO Orcus. Astron. Astrophys. 479, L13–L16.
Bauer, J.M. et al., 2002. The near infrared spectrum of Miranda: Evidence of crystalline water ice. Icarus 158, 178–190.
Binzel, R.P., 1988. Hemispherical color differences on Pluto and Charon. Science 241, 1070–1072.

Bonnet, H. et al., 2004. First light of SINFONI at the VLT. The Messenger 117, 17–24.
Brown, M.E., Calvin, W.M., 2000. Evidence for crystalline water and ammonia ices on Pluto's satellite Charon. Science 287, 107–109.
Brown, R.H., Cruikshank, D.P., Tokunaga, A.T., Smith, R.G., Clark, R.N., 1988. Search for volatiles on icy satellites. I – Europa. Icarus 74, 262–271.
Buie, M.W., Grundy, W.M., 2000. The distribution and physical state of H_2O on Charon. Icarus 148, 324–339.
Buie, M.W., Cruikshank, D.P., Lebofsky, L.A., Tedesco, E.F., 1987. Water frost on Charon. Nature 329, 522.
Calvin, W.M., Clark, R.N., Brown, R.H., Spencer, J.R., 1995. Spectra of the icy Galilean satellites from 0.2 to 5 μm: A compilation, new observations, and a recent summary. J. Geophys. Res. 100, 19041–19048.
Carry, B. et al., 2011. Integral-field spectroscopy of (90482) Orcus-Vanth. Astron. Astrophys. 534, 1–9.
Clark, R.N., Roush, T.L., 1984. Reflectance spectroscopy – Quantitative analysis techniques for remote sensing applications. J. Geophys. Res. 89, 6329–6340.
Clark, R.N., Carlson, R., Grundy, W., Noll, K., 2013. Observed ices in the solar system. In: Gudipati, M.S., Castillo-Rogez, J. (Eds.), The Science of Solar System Ices, Astrophysics and Space Science Library, vol. 356. Springer Science+Business Media, New York, p. 3, ISBN 978-1-4614-3075-9.
Cook, J.C., Desch, S.J., Roush, T.L., Trujillo, C.A., Geballe, T.R., 2007. Near-infrared spectroscopy of Charon: Possible evidence for cryovolcanism on Kuiper Belt objects. Astrophys. J. 663, 1406–1419.
de Bergh, C., Delsanti, A., Tozzi, G.P., Dotto, E., Doressoundiram, A., Barucci, M.A., 2005. The surface of the transneptunian object 90482 Orcus. Astron. Astrophys. 437, 1115–1120.
DeMeo, F.E. et al., 2010. A search for ethane on Pluto and Triton. Icarus 208, 412–424.
Dumas, C. et al., 2007. Surface composition of the largest dwarf planet 136199 Eris (2003 UB_{313}). Astron. Astrophys. 471, 331–334.
Dumas, C., Terrile, R.J., Brown, R.H., Schneider, G., Smith, B.A., 2001. Hubble space telescope NICMOS spectroscopy of Charon's leading and trailing hemispheres. Astron. J. 121, 1163–1170.
Dumas, C., Carry, B., Hestroffer, D., Merlin, F., 2011. High-contrast observations of (136108) Haumea. A crystalline water–ice multiple system. Astron. Astrophys. 528, 1–6.
Eisenhauer, F., et al., 2003. SINFONI – Integral field spectroscopy at 50 milli-arcsecond resolution with the ESO VLT. In: Iye, M., Moorwood, A.F.M. (Eds.), Society of Photo-Optical Instrumentation Engineers (SPIE) Conference Series, vol. 4841, pp. 1548–1561.
Fornasier, S., Dotto, E., Barucci, M.A., Barbieri, C., 2004. Water ice on the surface of the large TNO 2004 DW. Astron. Astrophys. 422, L43–L46.
Grundy, W.M., Buie, M.W., Stansberry, J.A., Spencer, J.R., Schmitt, B., 1999. Near-infrared spectra of icy outer Solar System surfaces: Remote determination of H_2O ice temperatures. Icarus 142, 536–549.
Grundy, W.M., Young, L.A., Spencer, J.R., Johnson, R.E., Young, E.F., Buie, M.W., 2006. Distributions of H_2O and CO_2 ices on Ariel, Umbriel, Titania, and Oberon from IRTF/SpeX observations. Icarus 184, 543–555.
Hapke, B., 1981. Bidirectional reflectance spectroscopy. I – Theory. J. Geophys. Res. 86, 3039–3054.
Hodapp, K.W. et al., 2003. The Gemini Near-Infrared Imager (NIRI). Publ. Astron. Soc. Pacific 115, 1388–1406.
Horne, K., 1986. An optimal extraction algorithm for CCD spectroscopy. Publ. Astron. Soc. Pacific 98, 609–617.
Jewitt, D.C., Luu, J., 2004. Crystalline water ice on the Kuiper Belt object (50000) Quaoar. Nature 432, 731–733.
Marcialis, R.L., Rieke, G.H., Lebofsky, L.A., 1987. The surface composition of Charon – Tentative identification of water ice. Science 237, 1349–1351.
Markwardt, C.B., 2009. Non-linear least-squares fitting in IDL with MPFIT. In: Bohlender, D.A., Durand, D., Dowler, P. (Eds.), Astronomical Society of the Pacific Conference Series, vol. 411, p. 251. <http://purl.com/net/mpfit>, <http://adsabs.harvard.edu/abs/2009ASPC.411.251M>.
Merlin, F. et al., 2010. Chemical and physical properties of the variegated Pluto and Charon surfaces. Icarus 210, 930–943.
Moore, M.H., Ferrante, R.F., Hudson, R.L., Stone, J.N., 2007. Ammonia water ice laboratory studies relevant to outer Solar System surfaces. Icarus 190, 260–273.
Strazzulla, G., Palumbo, M.E., 1998. Evolution of icy surfaces: An experimental approach. Planet. Space Sci. 46, 1339–1348.
Trujillo, C.A., Brown, M.E., Barkume, K.M., Schaller, E.L., Rabinowitz, D.L., 2007. The surface of 2003 EL_{61} in the near-infrared. Astrophys. J. 655, 1172–1178.
Verbiscer, A.J., et al., 2007. Simultaneous spatially-resolved Near-Infrared Spectra of Pluto and Charon. Lunar Planet. Sci. 38. p. 2318 (abstract).
Verbiscer, A.J., et al., 2008. Ammonia Hydrate on Tethys' Trailing Hemisphere. The Science of Solar System Ices (SCSSI): A Cross-Disciplinary Workshop (9064), LPI Contribution No. 1406.